JOURNAL OF GEOPHYSICAL RESEARCH, VOL. 111, D16207, doi:10.1029/2006JD007076, 2006

Single-particle measurements of midlatitude black carbon and light-scattering aerosols from the boundary layer to the lower stratosphere

J. P. Schwarz,[1,2] R. S. Gao,[1] D. W. Fahey,[1,2] D. S. Thomson,[1,2] L. A. Watts,[1,2] J. C. Wilson,[3] J. M. Reeves,[3] M. Darbeheshti,[3] D. G. Baumgardner,[4] G. L. Kok,[5] S. H. Chung,[1,2] M. Schulz,[6] J. Hendricks,[7] A. Lauer,[7] B. Kärcher,[7] J. G. Slowik,[8] K. H. Rosenlof,[1] T. L. Thompson,[1] A. O. Langford,[1] M. Loewenstein,[9] and K. C. Aikin[1,2]

Received 12 January 2006; revised 24 April 2006; accepted 16 May 2006; published 29 August 2006.

[1] A single-particle soot photometer (SP2) was flown on a NASA WB-57F high-altitude research aircraft in November 2004 from Houston, Texas. The SP2 uses laser-induced incandescence to detect individual black carbon (BC) particles in an air sample in the mass range of ~3–300 fg (~0.15–0.7 μm volume equivalent diameter). Scattered light is used to size the remaining non-BC aerosols in the range of ~0.17–0.7 μm diameter. We present profiles of both aerosol types from the boundary layer to the lower stratosphere from two midlatitude flights. Results for total aerosol amounts in the size range detected by the SP2 are in good agreement with typical particle spectrometer measurements in the same region. All ambient incandescing particles were identified as BC because their incandescence properties matched those of laboratory-generated BC aerosol. Approximately 40% of these BC particles showed evidence of internal mixing (e.g., coating). Throughout profiles between 5 and 18.7 km, BC particles were less than a few percent of total aerosol number, and black carbon aerosol (BCA) mass mixing ratio showed a constant gradient with altitude above 5 km. SP2 data was compared to results from the ECHAM4/MADE and LmDzT-INCA global aerosol models. The comparison will help resolve the important systematic differences in model aerosol processes that determine BCA loadings. Further intercomparisons of models and measurements as presented here will improve the accuracy of the radiative forcing contribution from BCA.

Citation: Schwarz, J. P., et al. (2006), Single-particle measurements of midlatitude black carbon and light-scattering aerosols from the boundary layer to the lower stratosphere, *J. Geophys. Res.*, *111*, D16207, doi:10.1029/2006JD007076.

1. Introduction

[2] Black carbon aerosol (BCA) is a by-product of incomplete combustion and is strongly connected to anthropogenic sources. In recent years the possible influences of BCA on climate forcing and atmospheric chemistry have been increasingly recognized [*Intergovernmental Panel on Climate Change* (*IPCC*), 2001; *Lary et al.*, 1999]. The contribution of BCA to radiative forcing is significant because BCA absorbs light efficiently and accumulates in the atmosphere [*Ogren et al.*, 1984; *Cooke and Wilson*, 1996; *Sato et al.*, 2003; *Penner et al.*, 1992; *Jacobson*, 2000; *Chung and Seinfeld*, 2005; *Koch and Hansen*, 2005]. Most BCA is removed from the troposphere via wet deposition with a lifetime of 5 to 10 days [*Kanakidou et al.*, 2005; *Chung and Seinfeld*, 2002]. BCA also contributes to indirect forcing of climate by acting as cloud condensation nuclei [*Lohmann et al.*, 2000; *Twohy and Poellot*, 2005]. A large fraction of BCA is expected to be in an internally mixed state in the atmosphere, which affects its nucleation and optical properties [*Möhler et al.*, 2005] and makes the quantification of BC loading and impact on climate difficult [*Clarke et al.*, 2004]. BCA mixing state has a direct role in BCA's global impact on temperature and precipitation. Internally mixed BCA likely involves sulfate and organic coatings because of the pervasiveness of these compounds in the free troposphere [*Murphy et al.*, 1998]

[1] Chemical Sciences Division, Earth System Research Laboratory, NOAA, Boulder, Colorado, USA.
[2] Also at Cooperative Institute for Research in Environmental Sciences, University of Colorado, Boulder, Colorado, USA.
[3] Department of Engineering, University of Denver, Denver, Colorado, USA.
[4] Centro de Ciencias de la Atmosfera, Universidad Nacional Autonoma de Mexico, Ciudad Universitaria, Mexico City, Mexico.
[5] Droplet Measurement Technologies Inc., Boulder, Colorado, USA.
[6] Laboratoire des Sciences du Climat et de l'Environnement, Gif-sur-Yvette, France.
[7] DLR-Institut für Physik der Atmosphäre, Oberpfaffenhofen, Wessling, Germany.
[8] Department of Chemistry, Boston College, Chestnut Hill, Massachusetts, USA.
[9] NASA Ames Research Center, Moffett Field, California, USA.

0148-0227/06/2006JD007076$09.00

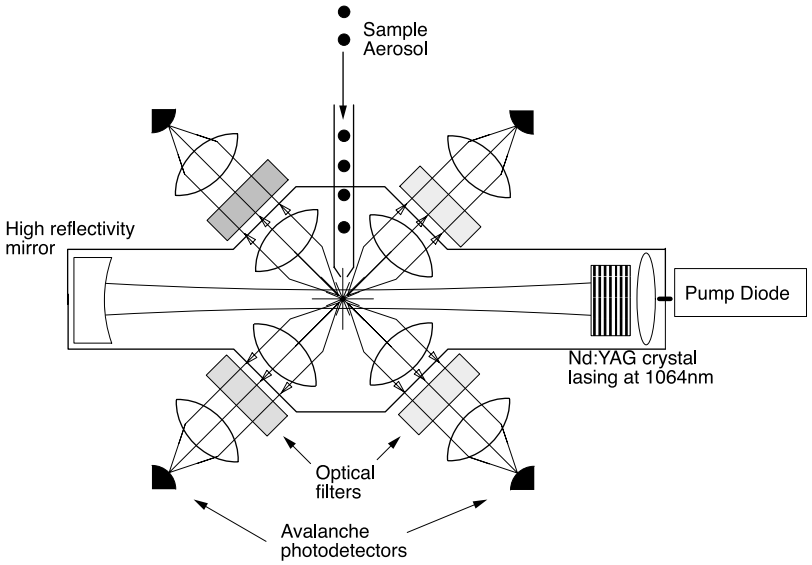

Figure 1. Schematic of the SP2 optical head showing the sample aerosol capillary, laser components, detection optics, and detectors. Four avalanche photodiode detectors (APDs) are focused on the intersection of the aerosol jet and the intracavity laser beam. Although it is drawn as parallel, the axis of the aerosol jet is perpendicular to the plane containing the APDs and optical detection axes. The light reaching the APDs is filtered to allow detection of specific wavelength bands of light. Two bands of visible light are used to derive the boiling point temperature of incandescing particles, and scattered laser light is used to size nonincandescing aerosols in high-gain and low-gain detectors.

and the favorable thermodynamics of organic phases [*Marcolli et al.*, 2004]. In the upper troposphere/lower stratosphere (UT/LS) measurements that unambiguously identify and quantify BCA are sparse, and dominated by one type of apparatus: wire impactors (WI) [*Blake and Kato*, 1995; *Pueschel et al.*, 1992; *Strawa et al.*, 1999]. Measurements using alternative detection techniques such as presented here can be expected to provide important additional constraints on the BCA burden and its mixing state in the free troposphere and lower stratosphere.

[3] Here we present measurements made with a new instrument, the Single Particle Soot Photometer (SP2) (Droplet Measurement Technologies (DMT), Boulder, Colorado), which has previously been used to measure BCA [*Baumgardner et al.*, 2004]. The SP2 uses laser-induced incandescence to quantify BCA. In this technique, described by *Stephens et al.* [2003], light-absorbing refractory aerosol is heated to vaporization by an intense laser beam. Refractory materials have high enough boiling point temperatures that they emit significant visible thermal radiation (''incandescent light'') as they vaporize. This radiation is characteristic of the composition and mass of the refractory component of the particle. Black carbon is expected to be the predominant refractory absorbing aerosol in the atmosphere. Particles that do not absorb enough energy to heat significantly are sized on the basis of the amount of light that they scatter out of the laser beam. These particles are referred to herein as ''scattering'' particles or aerosols (SA). In the current SP2 configuration, incandescent particles are sized in the range of 3–300 fg/particle (0.15–0.7 μm volume equivalent diameter for 1.42 g cm^{-3} density) and SA in the size range of 0.17–0.7 μm diameter. For some BC particles, the SP2 provides evidence of internal mixing through a comparison of the scattered light and incandescent light signals. In the material presented here, we (1) describe results from laboratory evaluations of the SP2 instrument addressing its ability to accurately count and size BCA and distinguish it from other incandescing aerosols, and to assess its sensitivity to instrument parameters such as laser intensity, sampling pressure, and alignment errors; (2) describe the flight instrument developed for the unheated and unpressurized payload bay of a NASA WB-57F high-altitude research aircraft; (3) present flight profiles of BCA and SA obtained from near the surface to 18 km from two flights covering latitudes 28–38°N, with information about the BCA mixing state; (4) present a comparison of the SP2 data set with previous measurements and global aerosol models; and (5) discuss the radiative forcing implications of these measurements.

2. SP2 Technique

2.1. Apparatus and Principle of Detection

2.1.1. SP2 Optical Head

[4] The basic measurement principles and experimental setup of the SP2 have been described previously [*Stephens et al.*, 2003; *Baumgardner et al.*, 2004]. The optical head of the SP2 is schematically shown in Figure 1. An air jet containing sample aerosol intersects an intense (~1 MW cm^{-2}), Nd:YAG, intracavity, continuous laser beam (λ = 1.06 μm) pumped by a diode laser. The laser is in a TEM00 mode, with a Gaussian intensity distribution. Four complex lenses are positioned to each capture a solid angle (~π/2 sr) of light emitted or scattered by particles in the laser beam, and image it onto an avalanche photo-detector (APD). All four detectors are synchronously sampled at 5 MHz. The APDs are optically filtered to detect different wavelength bands of

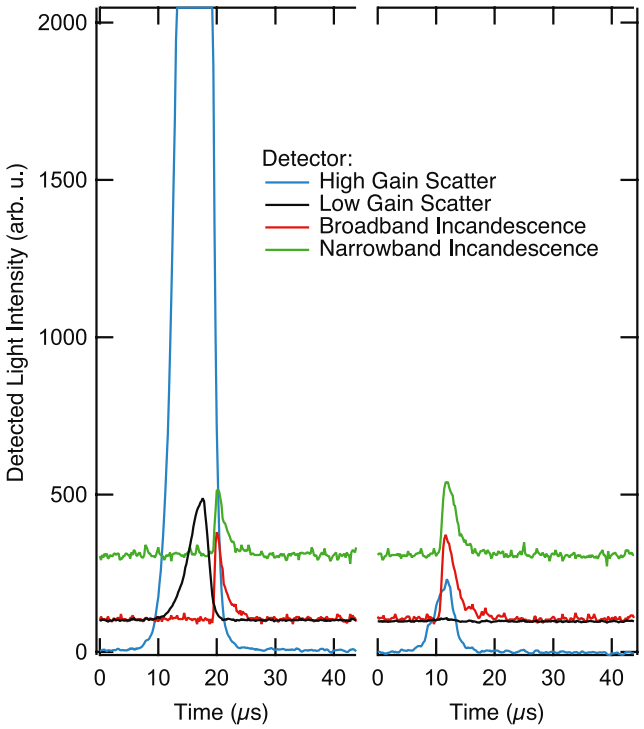

Figure 2. APD detector signals versus time for two BC particles detected in ambient air samples during a flight. The particles contain similar amounts of BC (~12 fg) as evidenced by similar broadband and narrowband incandescence signals. However, the scattering signals are different, indicating that the BC is in different mixing states. The particle on the right is considered externally mixed, i.e., a pure BC particle, because the scattering signal is comparable to that found with pure-BC particles of equivalent mass in laboratory tests. The particle on the left is considered internally mixed, i.e., contains a coating, because of the larger scattering signal. The time dependence shows that the coating is vaporized (the large scattering signal vanishes) before the BC core begins to incandesce. In contrast, the scattering and incandescence peaks are coincident for the externally mixed particle.

radiation. Two of the detectors sense a wavelength band of ~850–1200 nm at two different gain settings, and are used to optically size nonincandescing aerosols that only scatter laser light. These particles traverse the width of the laser beam (~1 mm over which the laser intensity is greater than 5% of its peak) in approximately 30 μs, generating a Gaussian response (in time) in each detector. The two other APDs detect incandescent light over either a "broadband" (~350–800 nm) or "narrowband" (~630–800 nm) wavelength interval and are used to characterize incandescing particles. The detector responses to incandescent particles are non-Gaussian in time. As an example, Figure 2 shows the incandescent and scattering signals for two BCA-containing particles detected during a sampling flight.

2.1.2. Selective Detection of Black Carbon

[5] In the aerosol community, the term "black carbon" (BC) has different meanings depending on the context of the discussion, and the method of detection. It is common to associate the meaning of measurements of carbonaceous aerosol components with the specific instrument being used [*Pöschl*, 2002]. The SP2 detects only the refractory and strongly light-absorbing component of combustion-generated aerosols. This component is referred to as either elemental carbon (EC) or BC depending on whether particles are being classified by their thermochemical or optical properties, respectively. Thus EC and BC are often used interchangeably. Here we label the ambient SP2 measurements as black carbon aerosol (BCA), recognizing that BCA represents only a component of the carbonaceous material often called soot. Soot, as a by-product of incomplete combustion, generally includes, in addition to BC, nonrefractory constituents including polycyclic aromatic hydrocarbons and aliphatic hydrocarbons.

[6] In the SP2 laser beam, light-absorbing refractory particles such as BCA absorb energy and are heated to their boiling point or vaporization temperatures, emitting thermal (incandescent) radiation that typically peaks in the near infrared. In our conceptual framework, once reaching its boiling point the particle is vaporized over time until its size is below the detection limit of the SP2 (~0.15 μm diameter). Laboratory tests showed that pure BCA spheres of sizes up to 1-μm diameter shrink below the detection limit before exiting the laser beam, confirming that detectable BC particles reach their boiling point temperature in the laser beam. The peak intensity of the incandescent light is proportional to the refractory mass of the particle, and the ratio of the broadband to narrowband detector signals from monitoring this radiation is related to the boiling point temperature of each particle and, thereby, constrains particle composition. Because the response of the SP2 to black carbon and other aerosols was empirically determined (discussed below), we do not require information about the actual boiling point of an incandescent material. However, as a conceptual convenience a simple numerical model was developed to translate the broadband/narrowband response ratio into an absolute temperature, allowing discussion of particle boiling point temperatures independently of the instrument-specific response ratio. The broadband-to-narrowband ratio of radiation emitted by a blackbody with unit emissivity was calculated as a function of temperature using the Planck function adjusted with the filter transmission properties and detector sensitivities. The relationship between the broadband/narrowband response ratio and temperature is near-linear for temperatures below 5000 K. The theoretical detector ratio was then compared to the measured ratio to estimate the boiling point temperature of individual particles. In this paper, the measured broadband-to-narrowband ratios are presented as boiling point temperatures.

[7] For a refractory particle to incandesce it must have a boiling point temperature high enough to emit measurable amounts of visible radiation and it must absorb light efficiently enough to reach those high temperatures. To test the likelihood that the SP2 response to BCA is unique among atmospheric aerosols, we nebulized a variety of materials in water and ethanol, and measured the SP2's characteristic response to each one. Powdered inorganic materials tested include nickel, chromium, chromium (III) oxide, vanadium, vanadium (V) oxide, iron, iron oxide, aluminum, synthetic seawater, sulfuric acid, niobium, and

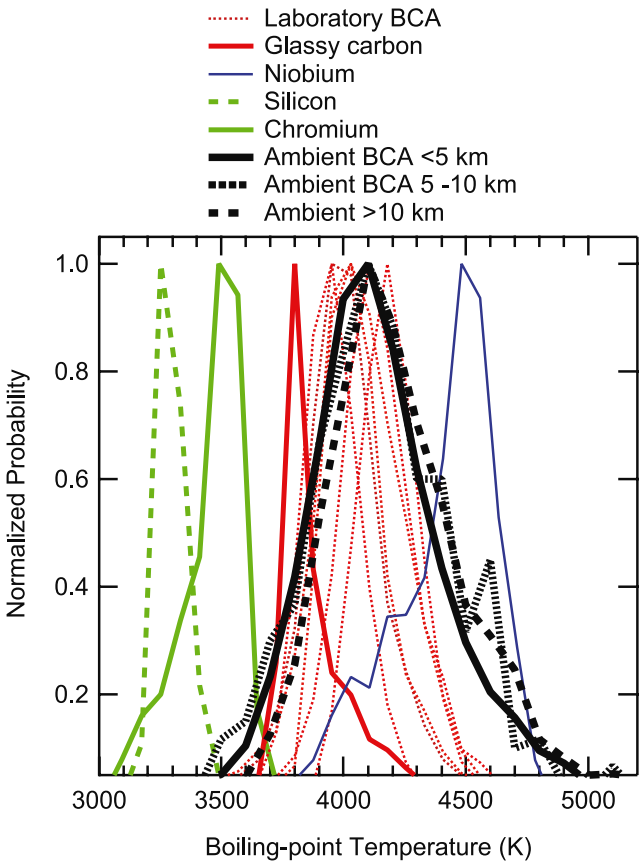

Figure 3. Normalized probabilities of boiling point temperatures as measured by the SP2 for aerosol populations observed in the laboratory and in the atmosphere during the two WB-57F flights. The curves are normalized by the peak occurrence for each data set. Individual laboratory data sets are shown for silicon, chromium, and niobium particles. Seven data sets are shown for commercial BC samples (red lines) (see text for details). Glassy carbon (solid red) is used as a reference material for testing the relative gains of the two incandescence channels. Data for ambient particles are divided into three groups on the basis of sampling altitude. The range and peak probability temperatures of the ambient particle groups are similar to those of the laboratory BC samples, indicating that all ambient incandescing particles contain BC. The large widths of the ambient particle distributions result from low signal-to-noise ratio for most of the ambient particles detected.

silicon (all supplied by Alpha Aesar, Inc., Ward Hill, Massachusetts). Aerosolized organic materials tested included tocopherol, olive oil, sucrose, and humis (tea). Eight different BCA types were also tested: Aquadag (Aecheson Colloids Company, Port Huron, Michigan), activated carbon, microcrystalline graphite, fullerene soot, glassy carbon, colloidal graphite (all supplied by Alpha Aesar, Inc., Ward Hill, Massachusetts), glassy carbon (Tokai Carbon Co., LTD., Japan), and flame-generated soot [*Slowik et al.*, 2004].

[8] In our laboratory tests few materials (including tungsten, aluminum, silicon, chromium, and niobium) other than BCA incandesced, and no nonincandescing aerosol showed any evidence of vaporizing in the laser beam. Figure 3 shows the characteristic boiling point temperatures for some of the incandescing materials, as measured by the SP2 in the laboratory. The range that we associate with BCA, ~3700–4300 K based on this figure, does not overlap significantly with the peak temperature of any other material that we tested. This range is also consistent with the wide range of temperatures for black carbon existent in the literature. Our laboratory tests suggest that the SP2 is strongly selective of BCA in an atmospheric air sample. The range of boiling point temperatures for the BCA samples is evidence that more than carbon composition affects the SP2 response. It is easy to speculate that crystal or amorphous structure, or impurities play some role in measured BCA temperatures. With further study it may be possible to discriminate between different sources of ambient BCA using systematic differences in boiling point temperature.

[9] Our translation of the broadband/narrowband response ratio into temperature assumes wavelength-independent emissivity for incandescing particles in the SP2. To test this assumption we measured the thermal radiation spectra of BCA, silicon, and chromium aerosols using a spectrometer linked by a fiber-optic to an SP2 detector location. The spectra were averaged over many thousands of individual particles to achieve useful signal-to-noise ratios. These measurements produced three interesting results. First, it showed that deviations from ideal blackbody radiation over 370 to 750 nm for all three incandescing materials are small. This suggests that simple models of blackbody radiation may be used to scale the incandescence signal calibration (section 2.2.2) to different materials. Second, the absolute boiling point temperatures derived from the spectroscopic analysis were in reasonable (±300 K) agreement with those generated by our simple model. Third, for the BCA samples, the C_2 (0,0) Swan band line at 516.5 nm was observed (indicating the presence of C_2 [*Harilal et al.*, 1997]), thereby confirming the possibility of using the SP2 for unambiguous identification of BC composition.

2.1.3. Detection of BCA Mixing State

[10] Features of particle scattering and incandescence signals from laboratory and atmospheric BCA have been analyzed for information about the mixing state of BCA. At present we make no attempt to differentiate coatings from other types of internal mixing, and our analysis is restricted to a qualitative assessment of the mixing state based on two parameters. The first is the time delay between the occurrence of the peak scattering signal and the peak incandescence signal. This delay is interpreted as an approximate measure of the time required to vaporize the coating, and we refer to it as the "coating vaporization time." Until the coating is vaporized (except for very thick coatings), the BC core is prevented from reaching its boiling point temperature by heat transfer to the coating. The second parameter is the ratio of the peak scattered light intensity to the peak broadband incandescent intensity (arbitrarily scaled). For an uncoated BC core this "peak ratio" is dependent on particle size, which determines the relative intensities of scattered and thermally emitted light. The presence of a coating on the core can only lead to increases in the ratio. Thus

increases in the peak ratio from its baseline value can be used as a proxy for coating thickness.

[11] In our conceptual model the sampling of an internally mixed BC particle is evidenced by a large time delay and an increase in the baseline scattering/incandescence ratio over that of uncoated BCA. Laboratory tests and theoretical studies support this qualitative relationship [*Moteki et al.*, 2005; J. G. Slowik et al., Intercomparison of instruments measuring black carbon content and optical properties of soot particles, submitted to *Aerosol Science and Technology,* 2006, hereinafter referred to as Slowik et al., submitted manuscript, 2006]. Examples of the SP2 signals from two ambient particles assumed to be coated and uncoated, but containing the same amount of BC, are shown in Figure 2. The equal amplitudes of the broadband incandescence peaks indicate the equivalence of the BC mass in each particle. In Figure 2 (left), the majority of scattered light ends before the particle starts to incandesce and the scattering signal is very large. These features indicate that a significant source of scattering cross section is removed before the onset of BC incandescence. In contrast, the scattering and incandescence signals in Figure 2 (right) are nearly coincident in time and the scattering signal is small. In this case, the particle is assumed to have little or no coating associated with it.

2.2. Signal Calibration

2.2.1. SP2 Optical Alignment

[12] A proper optical alignment is a cornerstone for correctly sizing aerosols and determining boiling point temperatures with the SP2. Misalignments can change both the response of the SP2 to a given particle, as well as its particle-to-particle response stability. For example, as a first alignment step, the SP2 instrument as provided by the manufacturer was modified to add an off-axis tilt to the optical filters in each detection axis. This eliminated light that reflected off of a filter into the opposing APD, causing errors in broadband/narrowband ratio and particle sizing. As a second step, the optimal position of each APD was confirmed. Signals from each detector were compared to those of a stationary detector, as the former was rastered over a small volume containing the image of the laser beam and aerosol jet. In the plane perpendicular to the detection axis, the gain profile of the active area (1.5 mm^2) of each detector was mapped out and the optimal position determined within 0.1 mm. The range of acceptable positions is on the order of ±0.3 mm. The APD position along the detection axis was chosen to slightly defocus the particle image in order to avoid locally saturating the detector gain medium, thereby causing a nonlinear response of the detector to scattered or incandescent light intensity. The scattered light detector positions were optimized on the basis of the quality of the Gaussian signal shape and the detector gain at the Gaussian peak (both measured for polystyrene latex spheres). For incandescing channels the average gain over the entire spatial extent of the incandescing image was maximized (using polydisperse BCA).

2.2.2. Black Carbon Mass Calibration

[13] We define the SP2 response to a BC particle as the peak signal intensity it induces in the broadband incandescence detector. The interpretation of this response is based on a key assumption: that the peak power of thermal radiation emitted by a small (<1 μm equivalent diameter) pure BC particle is linearly proportional to the mass of the particle's refractory component. This assumption was validated in a dedicated laboratory study using flame-generated soot of different sizes and fractal dimensions. In the study flame-generated soot with and without additional organic coatings was analyzed for fractal dimension, total particle mass, and organic mass fraction with an Aerodyne Aerosol Mass Spectrometer (AMS) operated in conjunction with a Scanning Mobility Particle Sizer (SMPS) [*Jayne et al.*, 2000; *Slowik et al.*, 2004; E. S. Cross et al., Aerosol particle density determination using light scattering in conjunction with mass spectrometry, manuscript in preparation, 2006]. BCA mass was determined indirectly from the difference between the total and organic particle mass. Using the AMS/SMPS results, a BCA intercomparison was conducted using two SP2 instruments, a Photoacoustic Absorption instrument [*Arnott et al.*, 1999], and a MultiAngle Absorption Photometer [*Petzold et al.*, 2002] in May 2005 (Slowik et al., submitted manuscript, 2006). A common manifold distributed a monodisperse BCA sample to each instrument over a range of mass-per-particle and fractal dimension. The results confirm a near-linear relationship between black carbon mass and SP2 response for black carbon particles of fractal dimension in the range 1.6 to 3 and mass in the range of 2–30 fg/particle. The fractal dimension range covers that estimated for ambient black carbon in the upper troposphere and lower stratosphere [*Jullien et al.*, 1987]. BC particles were also sampled after liquid (oleic acid) and solid (anthracene) organic coatings up to 100-nm thick were added. The coatings did not affect the BC mass calibration, indicating that they vaporized in the intense laser beam of the SP2 without interfering with the detection of the BC particle core or undergoing significant conversion into refractory carbon.

[14] Further validation of the linear mass-response assumption was provided by laboratory tests using a commercially available spherical BCA standard (glassy carbon spherical powder, Alpha Aesar, Inc., Ward Hill, Massachusetts). A flow of particles with known mass was formed using the manufacturer's specified density in conjunction with an electrostatic sorter to select a given particle diameter (0.3–0.8 μm diameter). In this measurement, the SP2 response is linear with particle mass to within a standard deviation of ±15%. This type of calibration, which was used to size all ambient BCA particles, is only valid for aerosols with the same boiling point temperature as the standard particles, because thermal radiative power, which determines the peak SP2 signal, is proportional to temperature to the fourth power.

[15] It follows from the assumptions about sizing of BCA that, since the thermal radiation is representative only of the mass and boiling point temperature of a particle, mass and temperature determinations are largely independent of laser intensity above a threshold value. Laboratory tests support this conclusion by showing that, with a factor of 3 reduction in laser power, mass determinations change by less than 30% for the largest mass particles (~800 fg/particle) tested and show virtually no change for small particles (<50 fg/particle). Boiling point temperature determinations are also highly insensitive to laser power over the same range. For the flights presented here, the laser was sufficiently intense to bring every particle of calibration BCA to

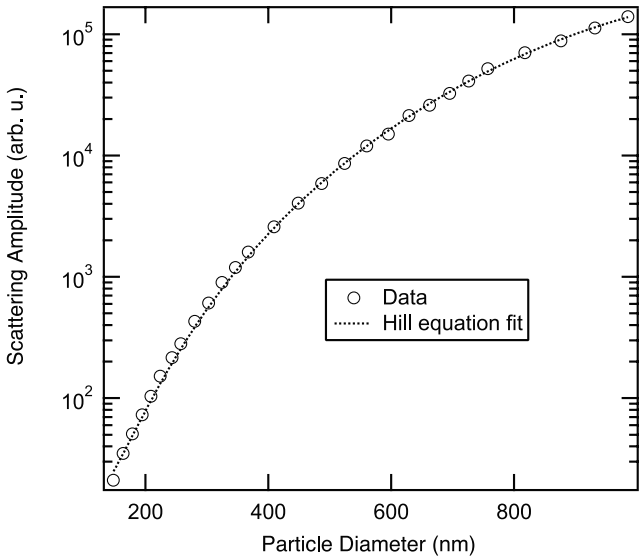

Figure 4. Scattering amplitude of dioctyl sebacate aerosol versus size as measured with the SP2. The aerosol was size selected with an electrostatic sorter. The fitting function was a Hill equation.

full incandescence, which is assumed to be the boiling point temperature. However, it is not yet clear if, and to what extent, coatings might affect the lower-size detection limit of the SP2. For example, coatings might prevent incandescence in particles with small BC mass fractions by conducting heat from the BC core. In the future a lower limit might be obtained for this effect by examining the data for the non-Gaussian scatter signals that might result from the incomplete vaporization of a coating.

2.2.3. Scattering Mass (Nonincandescent) Calibration

[16] The size of scattering aerosols was determined from the amplitude of their scattered light signals. Amplitudes were calibrated using dioctyl-sebacate particles size selected with an electrostatic sorter as shown in Figure 4. Dioctyl sebacate was chosen because it has an index of refraction reasonably similar to dry sulfate, which is assumed to be the primary composition of ambient nonincandescing particles in the size range of the SP2. Nonsulfate scattering particles will be sized with an error that generally increases with the difference in refractive index from that of sulfate. Because ambient aerosol was heated to ~25°C before detection, the nonincandescing particle sizes reported here are characteristic of dry sulfate. BC particles are not included in the scattering or total mass values reported here because the additional mass is not significant (<few percent) throughout the data set.

2.2.4. Operational Calibration Procedures

[17] In addition to occasional BCA mass calibrations, two other calibration procedures were performed routinely during the flight operation phase of the SP2 in order to ensure data quality. First, polydisperse glassy carbon spherical particles were sampled before and after each flight to monitor the relative gain of the broad and narrow-band detectors. Inadvertent changes in relative gain will be interpreted as drifts in boiling point temperatures. These temperatures measured over a 3-week period of flights were stable to better than ±100 K and to better than ±50 K from one flight to the next. On the basis of the BCA temperature range shown in Figure 3, this stability level is considered satisfactory for identifying BCA.

[18] Second, changes in laser power were monitored by measuring the scattering amplitudes of monodisperse polystyrene latex spheres sampled before and after each flight. The modal peak height is used as a reference of laser intensity and the width of the distribution of peak heights is related to the width of the aerosol jet in the laser beam. Laser power was continuously monitored in flight by recording the intensity of laser light leaking from the optical cavity. During each flight laser power deviated by less than 10% from its median value. In between flights it was stable (without adjustment) to ±15%. A month-long test of system stability in the laboratory showed that sensitivity drift of the scattered light detectors is negligible compared to laser intensity changes.

2.2.5. Pressure Dependence

[19] Operation of the SP2 on an aircraft requires that the pressure in the optical head change with ambient pressure in order to maintain a constant volume flow of ambient air into the laser beam. The pressures during flight reached minimum values near 50 hPa. Consequently, the SP2 was evaluated in the laboratory over the range of 830–50 hPa. In this range boiling point temperature determinations were stable to ±40 K, BCA mass sensitivity was independent of pressure to better than 10%, and the aerosol jet did not move in the laser or change shape significantly. The fact that boiling point temperatures did not change, even as the partial pressure of oxygen changed by an order of magnitude, is an additional indicator that chemical reactions (i.e., combustion) between carbon and oxygen do not produce enough light to affect the detection of individual BC particles. This last result is consistent with the lack of large deviations from the ideal of the blackbody spectra discussed in section 2.1.2.

2.3. Aircraft Configuration

[20] The SP2 operated in the unheated and unpressurized fuselage bay of a NASA WB-57F high-altitude aircraft. To ensure proper operation of the instrument in these conditions, the instrument enclosure was thermally controlled to ~25°C and the flight computer and laser power supply were mounted in pressure-tight enclosures to aid cooling.

[21] The flight instrument used a passive near-isokinetic inlet (Figure 5) as developed by the Aerosol Group at the University of Denver (Denver, Colorado, USA). The inlet slows an ambient sample from the ~90–200 m s^{-1} speed of the WB-57F aircraft to ~3 m s^{-1} after the internal diffuser while preserving ambient aerosol mixing ratios [*Jonsson et al.*, 1995]. The combination of primary and internal diffusers reduces corrections for aspiration errors over the measured size range. Net aspiration coefficients are reasonably independent (<15% variation) of aircraft speed and ambient pressure throughout typical WB-57F flight profiles. An important feature of this inlet is its exit flowmeter, which, when calibrated in the laboratory and used in conjunction with aircraft data (true airspeed, pressure, temperature), can measure the mass flow into the inlet's primary diffuser. The derived mass flow is used to calculate the net sampling aspiration efficiency of the dual-diffuser

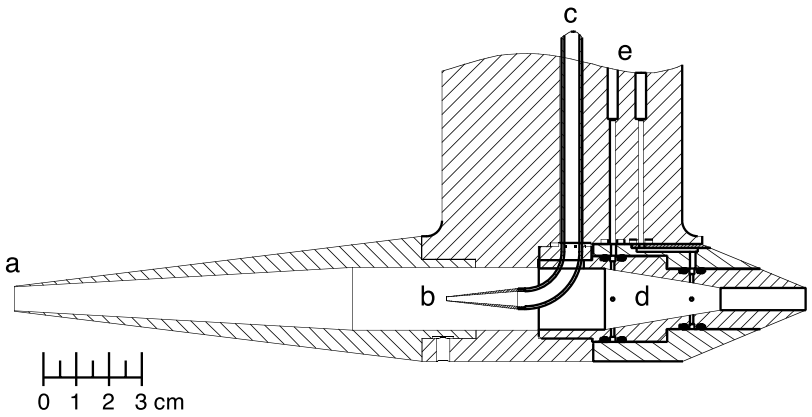

Figure 5. Schematic drawing of the passive, near-isokinetic inlet used for the SP2 on board the WB-57F aircraft. The inlet features are primary diffuser (indicated by a), internal diffuser (indicated by b), internal diffuser sample line (indicated by c), exit flowmeter (indicated by d), and differential pressure ports for the exhaust flowmeter (indicated by e). Air enters the primary diffuser and is slowed and heated by expansion. The diameter of the exhaust opening at the rear of the inlet body is chosen to limit the flow at the primary diffuser to maintain near-isokinetic sampling conditions. This flow is measured at the exit flowmeter using differential pressure. Similarly, the volume flow into the internal diffuser is controlled to maintain near-isokinetic sampling by a volume flow controller (downstream of the internal diffuser sample line, not shown).

configuration. During the flights presented here, measurements of the airflow through the external inlet body were not available and the actual aspiration efficiencies associated with the measurements could not be calculated. However, on the basis of the consistent performance of this inlet design on the WB-57F, estimated aspiration losses are less than 10% for particle sizes up to 0.50 μm sampled on the WB-57F flights. No corrections were made for sampling losses, but an additional 10% uncertainty is included in our analysis.

[22] Flow into the internal inlet diffuser was controlled with a volume-flow controller to be 40 volume cm^3 s^{-1} (vccs) over all aircraft altitudes and speeds. Approximately 4 vccs of this flow was isokinetically sampled, heated to ~25°C, and drawn through a laminar-flow element (LFE) to the SP2, where it was confined with sheath flow into a narrow jet of approximately one quarter of the laser beam diameter. The pressure in the optical head was servo-controlled to maintain a constant sample volume flow as measured by the LFE. The servo system controlled exhaust flow from the optical head using a pump and low pressure-drop valve. A small compressor and filter combination was used to produce aerosol-free air that was used as sheath flow and to purge the laser optics. Volume flow controllers (rather than mass flow) were used to control the sheath and purge flow in order to maintain good signal-to-noise ratios in the control circuits as ambient pressure decreased in flight. The sample temperature and pressure measured at the LFE were used to convert volume flow to mass flow.

[23] The aerosol transport efficiency between the internal-diffuser sample line and the SP2 detection volume within the optical head of the flight instrument was measured by comparison to a low-pressure condensation nuclei counter (CNC) [*Wilson et al.*, 1983]. Both detectors sampled particles from a common mixing chamber. Monodisperse dioctyl-sebacate particles in the size range 180–1000 nm diameter were added to the chamber and sampled by both instruments over the pressure range of 400–70 hPa. On the basis of known CNC losses of less than 10% under test conditions, SP2 transport losses at 70 hPa were larger than 10% only for particles larger than 700 nm diameter, increasing to 50% at 1000 nm diameter. Losses at pressures at and above 200 hPa were smaller than 10% for all sizes. The number and mass mixing ratios presented here have been corrected (<5%) on the basis of this calibration, scaling particle loss by Stokes number for pressures below 200 hPa and particle sizes greater than 700 nm.

2.4. Data Collection and Analysis

[24] During operation a high-speed digitizer continuously and simultaneously samples the signals from the four APD detectors at 5 MHz and stores them in a buffer. The computer reads the buffer, and finds particle detection events by searching the high-gain scattered light data. Each time the computer detects a light signal above a threshold value, it stores a time interval of data from all four detectors (Figure 2) for the entire time period that the particle was in the laser beam. The absolute time of each triggered event is also stored. These intervals of detector signals are stored unmodified for postflight analysis, and the remaining time series data are discarded. At high data rates the computer is not able to process all the buffered data, but does maintain a good measure of unprocessed or "dead" time. At altitudes above 4 km particle number concentrations were low enough that the dead time was less than 5%, but below 1 km the dead time approached 50%. Our results are corrected for dead time.

[25] In postprocessing, each particle is first categorized as "incandescent" if the signal-to-noise of the thermal radiation signal was high enough to calculate a boiling point temperature, and otherwise as "scattering" (SA). Scattering particles are assigned a diameter, while incandescing par-

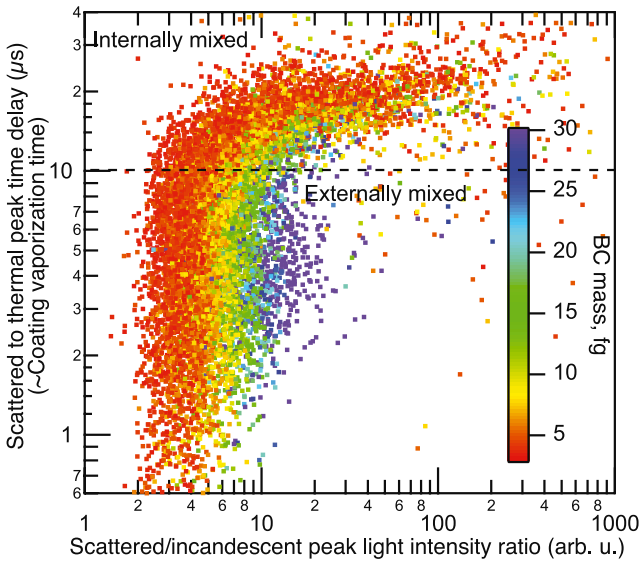

Figure 6. Correlation plot of SP2 signal diagnostics obtained from incandescing particles detected in ambient air during the 10 and 12 November flights. The diagnostics are used to distinguish internally from externally mixed BCA. The vertical axis is the time delay between the occurrence of the peak scattered light intensity and the peak incandescent light intensity. The largest time delays are caused by the times needed to vaporize thick coatings on BC particles, which interfere with the heating required to bring the BC mass fractions to incandescence. The horizontal axis is the ratio of peak scattered light intensity to peak incandescent light intensity (in arbitrary units). The ratio is used as a qualitative proxy for the coating thickness or ratio of non-BC to BC mass. All ambient data from the two flights are shown. Particles with delay times above 10 μs are considered to be coated. Those with shorter delay times are considered externally mixed. Because the sensitivity of this SP2 diagnostic to coating thickness is not known, the estimate of the internally mixed fraction is considered a lower limit.

ticles are assigned a boiling point temperature (based on the measured broadband/narrowband ratio). Particles identified as BCA by their temperature are also assigned a mass. The respective calibration procedures are discussed above.

[26] Once individual detection events are processed, they are binned to obtain BCA and SA ambient concentrations, typically for 30-s averaging periods. This primary output of the SP2 data analysis is then binned into 1-km altitude slices.

3. SP2 Results and Interpretation

[27] SP2 data were obtained on two WB-57F flights (10 and 12 November 2004) that covered a 10° range of longitude (88–98°W) and latitude (29–38°N), and reached altitudes of 18.7 km. Data were also obtained throughout the flights for CO [*Loewenstein et al.*, 2002], O_3 [*Proffitt and McLaughlin*, 1983], and pressure and temperature. Data taken in clouds (~5% of our data) were removed to avoid biases caused by the generation of particles from the impaction of large cloud particles with the inlet walls [*Murphy et al.*, 2004].

3.1. SP2 Incandescent Temperature Distribution

[28] Measured boiling point temperatures of incandescing particles were consistent with the BCA temperature range obtained in the laboratory. Plotted in Figure 3, in the context of the laboratory temperature calibrations, are the distributions observed in the altitude ranges 0–5 km (8770 particles), 5–10 km (420 particles), and 10–19 km (1910 particles). The large widths of the ambient distributions result from sampling a broad size distribution that includes many particles near the detection limit. The expected distribution width, calculated from a mathematical simulation of BCA temperatures including only the background instrument noise and a typical ambient aerosol mass distribution, matches the observed distribution width to within 40%. The single temperature distribution contrasts with the earlier findings of *Baumgardner et al.* [2004] in the Arctic stratosphere, which revealed, in addition to BCA, a second population of particles at a lower temperature. The composition of this additional population was assumed to be non-BC. The representativeness of the temperatures found in either region is not known. However, the signal analysis and calibration of the earlier data set were much less stringent than those presented here, introducing more uncertainty in the interpretation of the earlier study.

3.2. Internal Mixing With Black Carbon

[29] A qualitative assessment of the BCA mixing state for the aircraft data set was made using the approach described in section 2.1.3. The relationship between coating vaporization time and peak ratio is shown in Figure 6 for ambient BCA. Below a 10-μs coating vaporization time the peak ratio increases smoothly with particle mass over a range of delay times, establishing a relationship for peak ratio and uncoated BC core mass. In contrast, the results above a 10-μs delay show a positive correlation of coating vaporization time with the peak ratios, which increase by up to an order of magnitude. This correlation strongly indicates the presence of a coating on the sampled particles. These trends are consistent with those found in the laboratory SP2 study discussed by Slowik et al. (submitted manuscript, 2006). On the basis of Figure 6, we estimate that the SP2 cannot distinguish coatings on particles that exhibit a coating vaporization time of less than 10 μs. The number fraction of internally mixed BCA based on this estimate is approximately 40% for the particles observed on the two WB-57F flights. This value should be considered a preliminary estimate until more detailed tests are undertaken to determine the sensitivity of the SP2 to coated BCA.

3.3. SP2 Number and Volume Size Distributions

[30] The number and volume/mass size distributions for both SA and BCA are shown in Figures 7 and 8 and summarized in Table 1. SA number concentrations are shown for the size range of 0.17–0.67 μm. Figure 7 also shows a comparison of these values with results from the Focused Cavity Aerosol Spectrometer (FCAS) [*Jonsson et al.*, 1995] flown on board the WB-57F aircraft in 2003–2004. Shown are averages from approximately 500 FCAS size distributions (30-s averages) of dry particles between

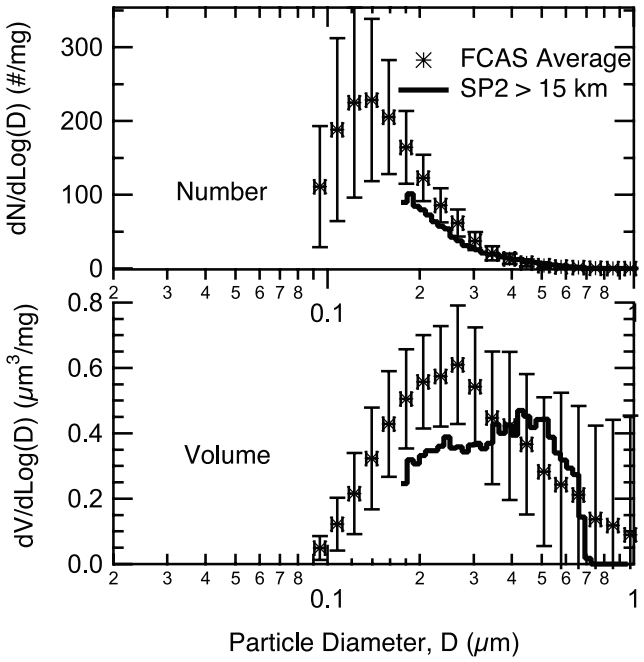

Figure 7. Number and volume distributions for scattering aerosol (SA) in the lower stratosphere obtained on the flights of 10 and 12 November. Data from the SP2 for altitudes above 15 km (lines) are shown along with results from the Focused Cavity Aerosol Spectrometer (FCAS) (markers). The FCAS distribution is an average of 534 profiles over the range of 60–100 hPa and 29–39°N latitude. The error bars are the sum of the standard deviations of profiles within the ensemble of profiles. These uncertainties represent an estimate of time-to-time and place-to-place variability of the FCAS profile data in the UT/LS, because the statistical uncertainty of each profile was small. Number and volume results are expressed per milligram (mg) of ambient air. At 15 km, approximately 0.2 mg of air occupies 1 cm^3. Approximately 200,000 SA particles were measured by the SP2 above 15 km.

0.1 and 1 μm diameter. The distributions were obtained in the upper troposphere and lower stratosphere (100–60 hPa) at midlatitudes (29–39°N) in several airborne campaigns. This range contains most of the volume of lower-stratospheric SA. The comparison shows that the SP2 SA results are typical for the lower stratosphere. To estimate the fraction of SA mass that was outside the detection range of the SP2, we compared the integrals of the FCAS and SP2 average size distributions to yield a scaling factor of 1.7. These values indicate that the SP2 detects approximately 60% of the total SA mass in the detection range of the FCAS. In the mass comparisons presented below, the SP2 scattering aerosol mass is scaled by a factor of 1.7. Contributions of coarse mode particles (mainly dust and sea salt), which typically become significant at and below ~900 hPa ambient pressure, are not accounted for with this factor.

[31] The lower BCA detection limit of the SP2 flight instrument was ~2 fg BC per particle (corresponding to a volume-equivalent pure-BC particle of ~0.150 μm diameter with density of 1.42 g cm^{-3}). For the results in Figure 8, only BCA of at least 3 fg/particle is included to avoid issues of detection efficiency and to simplify our analysis. The upper detection limit was ~300 fg/particle (~0.7 μm volume equivalent diameter). BC particles larger than this limit, which are detected but not sized, make up less than 0.05% of the ambient BCA number throughout the flights and, hence, are neglected in our analysis. To estimate the fraction of BCA mass that was below the size detection limit we assumed that the mass distribution of ambient BCA could be represented by a single lognormal distribution. Single lognormal distributions of BCA have been observed in the stratosphere by *Pueschel et al.* [1992] and in the free troposphere by *Clarke et al.* [2004].

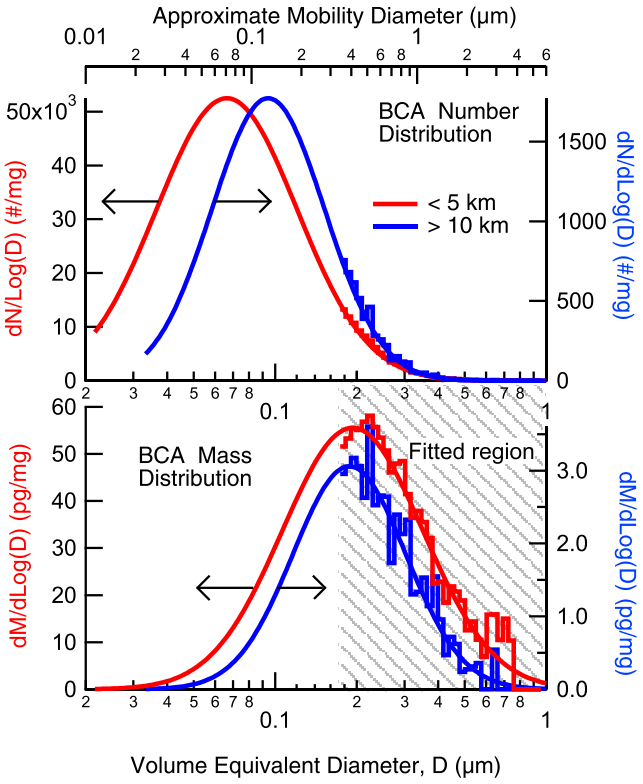

Figure 8. Number and mass distributions of BCA observed by the SP2 in two altitude ranges (below 5 km and above 10 km) on the flights of 10 and 12 November. The observed distributions are shown as histograms over the detection range of the SP2. Both mass distributions in the bottom plot are fit with a lognormal function over the size range highlighted by cross hatching. The number distribution fits implied by the lognormal mass fits are included in top plot. Note the range differences in the right and left vertical axes. Approximately 9000 BCA particles were measured below 5 km, and ~2000 above 10 km. The bottom horizontal axis represents the volume-equivalent diameter derived from the SP2 BC mass determination using a particle density of 1.42 g cm^{-3}. The top horizontal axis represents the mobility diameter of the BCA, which is based on a mass-to-mobility relationship taken from *Slowik et al.* [2004] for fractal flame-generated soot. Number and volume results are expressed per milligram (mg) of ambient air. At 10 km (5 km), approximately 0.4 (0.7) mg of air occupies 1 cm^3.

Table 1. Summary of Results

	Result
Black Carbon Aerosol (BCA)	
SP2 detection range	3–300 fg/particle (0.15–0.7 μm volume equivalent diameter)
MMR scaling factor[a]	1.7
MMR in the lower stratosphere	1.6 ± 1.6 ng kg^{-1} (70–200 hPa)
MMR range from wire impactor[b]	1.4–6.4 ng kg^{-1} (64 hPa)
Average mass (range) below 5 km[c]	42 ng kg^{-1} (6–135 ng kg^{-1})
Average mass (range) above 10 km[c]	1.6 ± 0.7 ng kg^{-1} (0.6–2.6 ng kg^{-1})
Scattering Aerosol (SA)	
SP2 detection range	0.17–0.7 μm diameter
MMR scaling factor[a]	1.7
MMR in the lower stratosphere	670 ± 270 ng kg^{-1} (70–100 hPa)
FCAS MMR[d]	562 ng kg^{-1} (60–100 hPa)

[a]The scaling factor was applied to all mass mixing ratio (MMR) data to account for mass outside the size limits of the SP2.
[b]Data for average stratospheric conditions from Table 3 of *Strawa et al.* [1999] adjusted to 19 km altitudes.
[c]Values include scaling factors. Values are average and range of 1-km binned averages shown in Figures 9a and 9b.
[d]Data from 524 distributions measured between 29–39°N during 2003–2004 with the Focused Cavity Aerosol Spectrometer (FCAS) [*Jonsson et al.*, 1995].

[32] SP2 BCA mass distributions are grouped into two altitude ranges and fit by monomodal lognormal functions as shown in Figure 8. The lower horizontal axis represents volume-equivalent diameter of BCA (i.e., the diameter of a solid spherical BC particle with the same mass as the detected particle). The upper axis shows estimated mobility size based on a mass-mobility diameter relationship observed for flame-generated fractal-BC particles [*Slowik et al.*, 2004]. Our mass distribution peaks in a size range that is quantitatively similar to mass distributions of BCA found in the free troposphere below 6 km [*Clarke et al.*, 2004], in the boundary layer [*Heintzenberg and Covert*, 1984], and in a polluted urban area [*Kondo et al.*, 2006]. All of those BCA distributions are approximately lognormal with a single peak near 0.1–0.2 μm diameter. The corresponding number distributions are also shown in Figure 8. The lognormal number distributions shown are derived from the lognormal fit to the mass distributions. On the basis of the fits to the present data set, approximately 60% of total BCA mass and 5% of total BCA number are detected by the SP2. The remaining mass and number are associated with particles below the size detection limit of the SP2. Thus, to estimate the total BCA mass, we increased the SP2 mass values by a scaling factor of 1.7 throughout the data set. This factor is unrelated to the scaling factor for scattering mass, which has the same numerical value only by coincidence. It is important to note that if significant BCA mass exists in one or more unidentified modes below the SP2 size limit, the scaling factor will be an underestimate.

3.4. Vertical Profiles of SP2 Mass Mixing Ratios

[33] The mass mixing ratios (MMR, mass of detected particles per unit mass of air) of both BCA and total aerosol (TA, the sum of BC and SA) are plotted in Figure 9a against pressure altitude. Global model results are also included in Figure 9a. The mass concentrations corresponding to the MMR values are shown in Figure 9b. The ratio of BCA to total aerosol mass is shown in Figure 10 and vertical profiles of CO and O_3 tracer gas mixing ratios are shown in Figure 11. Each measured data point represents a quantity averaged over 1 km of altitude from one flight. SP2 MMR values for both aerosol types include the factor of 1.7 to account for mass outside the respective size detection limits. The error bars are the sum (in quadrature) of the sample standard deviation, a 10% uncertainty for anisokinetic sampling errors, a 10% uncertainty for flow calibration, and 20% uncertainty in the mass calibration factor applied to both BCA and sulfate aerosols. The thermal tropopause varied between 120 and 200 hPa on the two flights, consistent with the inflection in the O_3 profile. Average values of CO near 100 parts per billion by volume (ppbv) or less indicate that the sampled tropospheric air masses are well-mixed background air rather than highly polluted air recently transported from the boundary layer.

[34] In the lower troposphere the MMRs of both aerosol types depend strongly on altitude. Above the boundary layer, TA and BCA mass fall off even more strongly with altitude. The rates of aerosol removal for the two types are not matched in this region of the atmosphere: the BCA mass fraction shows only a uniform decreasing gradient with pressure altitude. Near and above the tropopause, the SA MMR increases with altitude as the fraction of stratospheric air increases and the aerosol mass in the stratospheric sulfate layer is detected. The SP2 results indicate a near-constant MMR (within a factor of about 3) for BCA between 5 and 18 km, which includes the tropopause. This result suggests that the BCA net removal timescale in the observed size and altitude ranges is long compared to mixing times. Furthermore, the similarity of BCA size distributions above 10 km and below 5 km suggests that removal of BC particles is independent of their mass (Figure 8). No obvious geographic dependence was observed over the limited ranges of latitude and longitude sampled in these flights. The separate data points shown in Figures 9a and 9b for the two flights indicate the day-to-day variability in BCA and TA amounts. The largest differences for both are found in and below the middle troposphere. It is not clear if these results are typical of normal atmospheric variability.

[35] A range for wire-impactor measurements of BCA typical for the lower stratosphere is also included in

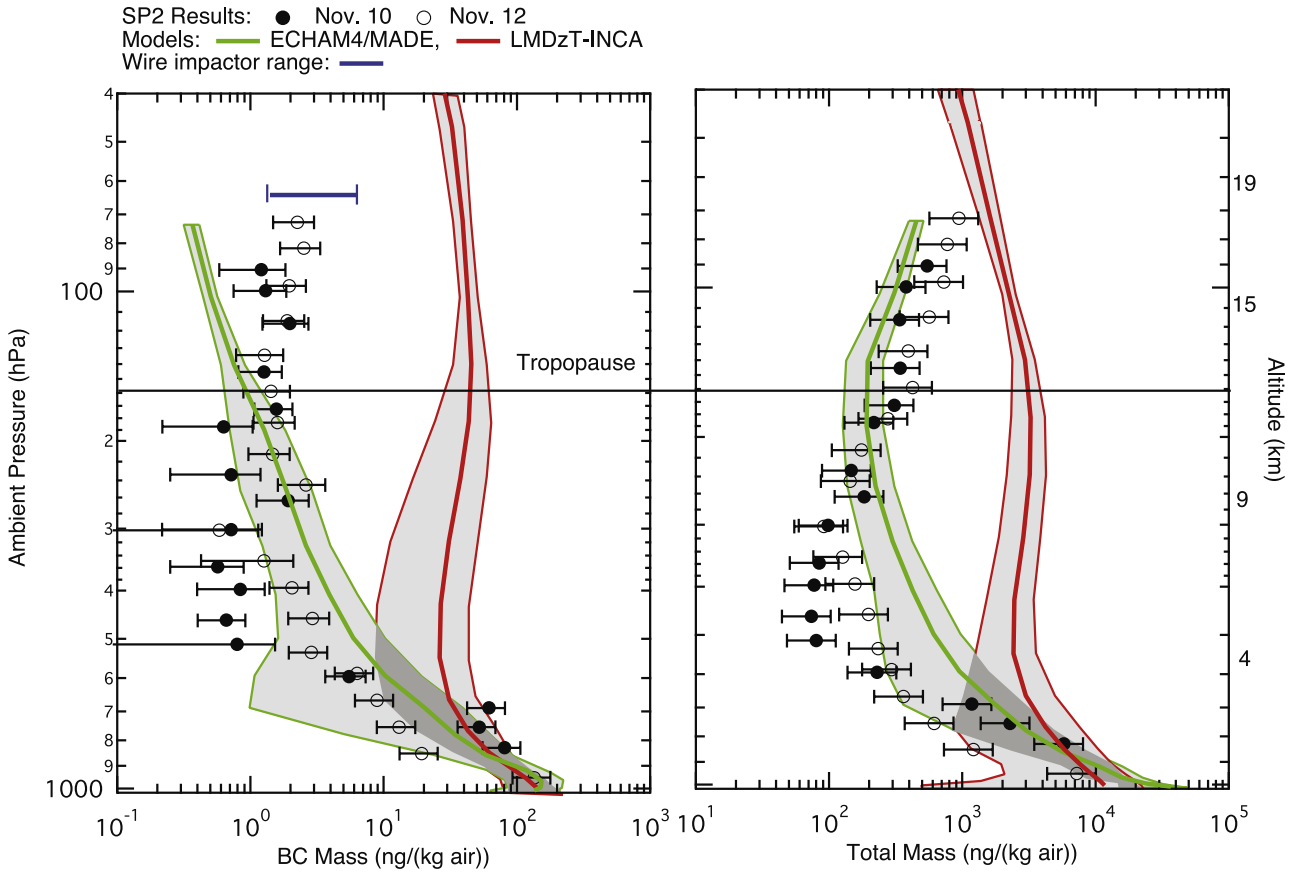

Figure 9a. Vertical profiles of (left) BCA and (right) total aerosol mass mixing ratios (MMR) in units of ng kg^{-1} air plotted against ambient pressure and approximate altitude (assuming a standard atmosphere). SP2 MMR values are shown in 1-km altitude bins for the flights of 10 November (solid circles) and 12 November (open circles). The values include the scaling factor of 1.7 over the entire profile to account for mass at sizes outside the SP2 detection range (see text discussion). The SP2 error bars represent sample variability and known uncertainties (see text discussion). A wire impactor range (blue line) is shown from *Strawa et al.* [1999]. Results for the LMDzT-INCA (red) and ECHAM4/MADE (green) models are shown as November averages for the geographic region of the SP2 flights. The shaded regions represent the model variability of the average values. In the case of ECHAM4/MADE, the model variability is identified with standard deviations calculated from all 12-hourly mean concentrations obtained for November. The thermal tropopause was observed to be near 150 hPa (horizontal black line) during the two flights. At 10 km (5 km), approximately 0.4 (0.7) kg of air occupies a volume of 1 m^3.

Figures 9a and 9b [*Strawa et al.*, 1999]. The present values are consistent with the lower end of the range. The only previously reported results from SP2 observations are those made in the lower stratosphere at high Arctic latitudes (60–90°N), which show average mass concentrations that range approximately 0.3 to 60 ng kg^{-1} [*Baumgardner et al.*, 2004]. At the lowest latitudes (~60–66°N) the Baumgardner et al. values are up to 30 times lower than at higher latitudes, and agree well with the midlatitude SP2 results shown in Figures 9a and 9b. The very high BCA mass fractions in the *Baumgardner et al.* [2004] results at higher latitudes are not observed in the present data set.

[36] BCA mass loadings in the latitude range explored here have also been reported by the Aerosol Robotics Network (AERONET) [*Schuster et al.*, 2005]. In North America, between 30 and 40°N, total column loadings were between ~0.3 and 3 mg m^{-2} BCA. The SP2 average column loading from 1 to 18 km (adjusted for undetected mass) was 0.2 ± 0.1 mg m^{-2}, clearly on the low side of AERONET values. Column measurements are dominated by the low-altitude BCA loading, which is generally highly variable because of proximity to BCA source regions.

4. Comparison With Aerosol Model Results

[37] The SP2 mass observations are compared with two global aerosol models in Figures 9a and 10. The first model is the ECHAM4 general circulation model (GCM). The ECHAM4 model was applied as described by *Hendricks et al.* [2004], but supplemented by the aerosol dynamics module MADE [*Lauer et al.*, 2005]. This enables predictions of the total aerosol number concentration and size distribution. The second model is the LMDzT GCM that includes the Interaction with Chemistry and Aerosols (INCA) module [*Guibert et al.*, 2005]. In addition to BCA, the ECHAM4/MADE (E/M) model includes sulfate/nitrate/

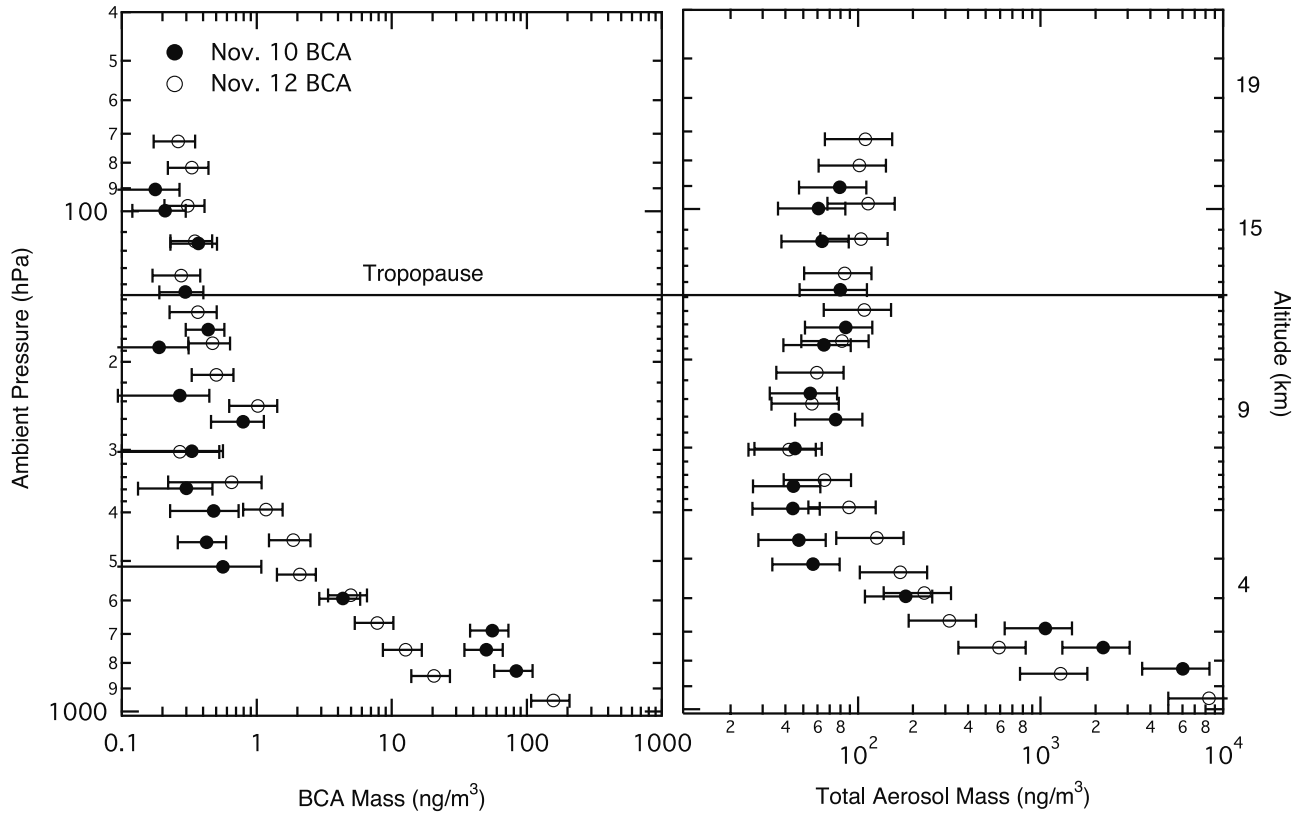

Figure 9b. Vertical profiles of (left) BCA and (right) total aerosol mass concentration in units of ng m^{-3} as a function of ambient pressure and approximate pressure altitude. Other details are the same as in Figure 9a.

ammonium and also particulate organic matter, sea salt, and dust, and the LMDzT-INCA (L-I) model includes sulfate, particulate organic matter, sea salt, and dust. Particle emission inventories representative for 2000 were used following the AeroCom recommendations [*Dentener et al.*, 2006]. Aircraft emissions were not taken into account. The contribution of aircraft emissions to large-scale BC and sulfate mass concentration probably is small [*Kjellström et al.*, 1999; *Hendricks et al.*, 2004]. The results shown for each model are averages for model grid boxes that include the narrow geographical range of the observations. The averages are monthly means (November) calculated from the 2000–2002 time period in the case of the L-I data and a 10-year climate simulation in the case of the E/M data.

[38] The global model results agree well (within an order of magnitude or better) for both TA and BCA below about 4-km altitude. Near the surface, differences in average BCA mass values are small. Above 4 km, the model mean values diverge for both aerosol types. Near the tropopause (about 12 km) BCA mass values differ by a factor of 50 and total mass values by about 20. The variability in both profiles is comparable in the two models. The model agreement near the surface in Figures 9a and 9b suggests that surface sources and sinks and near-surface aerosol processes are represented similarly in the models. Many factors could lead to the model differences above a few kilometers altitude in Figures 9a and 9b including the specific ways that the models represent vertical transport, wet removal, and BCA conversion from hydrophobic to hydrophilic.

[39] The E/M and L-I models are included in the AeroCom initiative designed to compare aerosol models with each other and with aerosol observations (http://nansen.ipsl.jussieu.fr/AEROCOM/data.html). The average fraction of BCA mass above 5 km from the 16 AeroCom models is 21% with a diversity of 52%. Diversity in this case is defined as the standard deviation of results normalized by the mean of the model group. The E/M value of global BCA mass above 5 km [15%] is near the low end of the overall range and the L-I value [37%] is near the upper end, qualitatively consistent with the differences in Figure 9a [*Textor et al.*, 2005].

[40] For BCA MMR, the observations agree well with the models near the surface (Figure 9a). The observations show a large gradient with altitude in the first 5 km above the surface and show little gradient at higher altitudes. Overall, the agreement with the E/M model is better than with the L-I model throughout the profile, since the latter shows a smaller gradient in the lowest altitudes. A similar comparison with the models is found for the measured mass fraction of BCA in Figure 10. The SP2 comparisons with MMR and mass fraction suggest that removal efficiencies in the L-I model might be too low. However, considering that the comparison is between a data set with limited spatial and temporal range and results from models with low spatial resolution (2–3° in latitude and longitude), different trans-

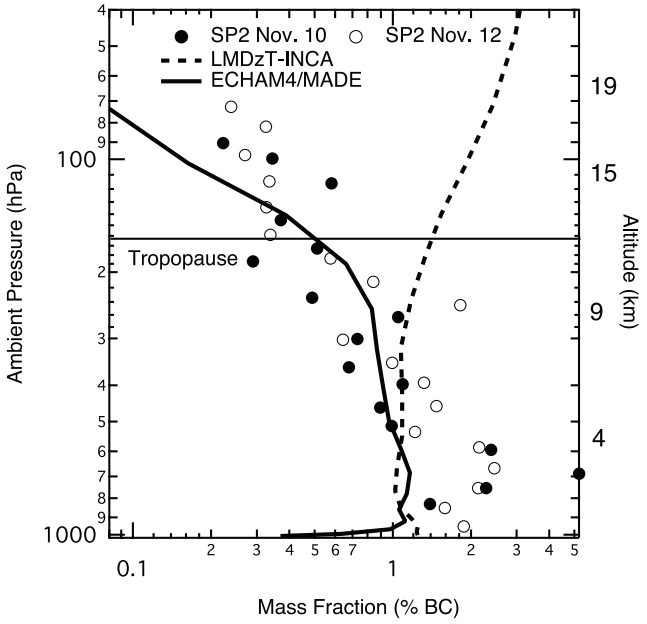

Figure 10. Vertical profiles of the BCA mass fraction as a function of ambient pressure and approximate pressure altitude for the observations (circles) obtained on the flights of 10 and 12 November. Data are averaged over 1-km altitude bins for each flight. Also shown are results from the ECHAM4/MADE (solid line) and LMDzT-INCA (dashed line) global aerosol models. The thermal tropopause was observed to be near 150 hPa (horizontal solid line) during the two flights.

port characteristics are also a likely cause of the differences in the model results.

[41] The comparison of observations of TA with the models shows similar features to the BCA comparison. The observations and models agree well near the surface, and throughout the profile, they agree significantly better with the E/M than the L-I model. The largest differences with the E/M results are in the middle troposphere where the observed values are significantly lower and outside the model variance. At lower altitudes, as the undetected coarse mode contributions from dust and sea salt become significant, the SP2 TA mass becomes an underestimate.

5. BCA Radiative Forcing Implications

[42] The measurements of BCA mass loading and its vertical distribution will ultimately improve the accuracy of radiative forcing (RF) estimates for anthropogenic activities. Anthropogenic BC emissions from fossil fuel and biomass burning contribute comparably to direct RF [*IPCC*, 2001]. The determination of the direct RF effect of BCA is sensitive to a number of factors, including the vertical distribution of BCA as provided by GCM calculations. For example, *Haywood and Ramaswamy* [1998] report that the direct RF of a BCA layer increases by approximately a factor of 5 as the layer is moved between the surface and 20 km in one GCM. Furthermore, clouds can increase the direct effect locally by as much as a factor of 10 depending on cloud properties and solar zenith angle. A similar effect is evident in the results of *Chung and Seinfeld* [2005]. As the altitude of an air mass increases, the RF sensitivity is enhanced from a combination of less scattering and absorption above the air mass with increased scattering of cloud layers below it. In a sensitivity study with one of the models used in the IPCC Assessment [*IPCC*, 2001], confining all BCA to the lowest 2 km of the model atmosphere decreased the global mean direct RF value by up to a factor of 2 [*Haywood and Ramaswamy*, 1998].

[43] The present results and model intercomparisons suggest that BCA mass might be overpredicted regionally and perhaps globally above 5 km in many aerosol models. However, the consequences for anthropogenic RF calculations are likely bounded within a factor of two on the basis of the sensitivity noted above. Future measurements with the SP2 and other instruments will add confidence and detail to these assertions and lead to model improvements. Of high value will be measurements in polar regions where BCA mass loadings have an enhanced RF contribution because of high average surface albedo.

6. Conclusions

[44] We have constructed, tested, and operated a new flight instrument, the SP2, for measuring black carbon

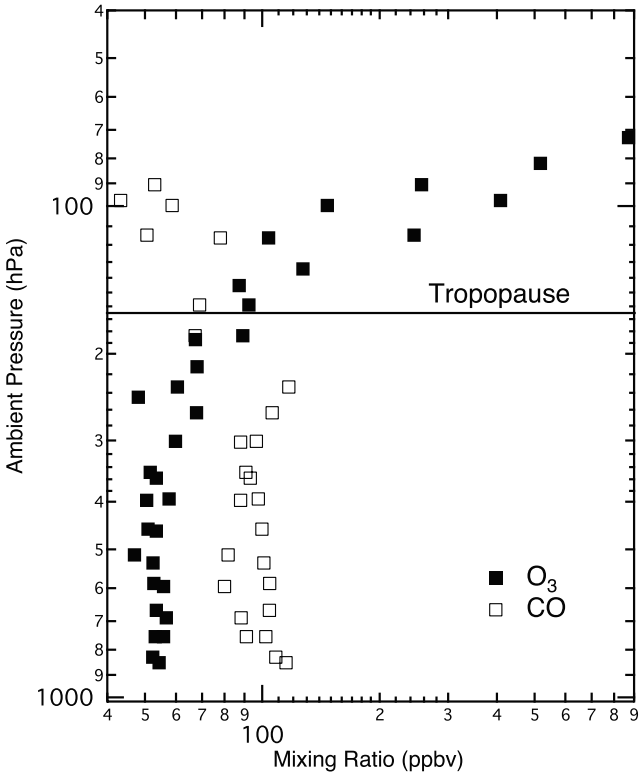

Figure 11. Vertical profiles of carbon monoxide (open squares) and ozone (solid squares) mixing ratios as a function of ambient pressure and approximate pressure altitude as obtained on the flights of 10 and 12 November. Data are averaged over 1-km altitude bins for each flight. The thermal tropopause was observed to be near 150 hPa (horizontal solid line) during the two flights.

aerosol (BCA). The SP2 uses laser-induced incandescence to detect and size individual BC particles. The SP2 also detects and sizes nonincandescing particles with the assumption of dry sulfate composition. We have characterized the SP2 response to a wide variety of laboratory-generated aerosols, including BCA, and have identified a range of boiling point temperatures that we believe is unique to BCA in the atmosphere. The SP2 was also tested in the laboratory to explore its detection limits, sampling biases, sampling efficiency, pressure dependence, and sensitivity to alignment errors. A separate study cited here established that the SP2 sensitivity to black carbon mass is independent of coatings and particle morphology.

[45] Benefits of the laser-induced incandescence technique include the following: real-time detection and characterization of individual BC particles, sensitivity to the BCA mass and coating of each particle, and suitability for continuous particle measurements from the surface to the lower stratosphere on board aircraft. Additionally this technique lends itself to laboratory quantification of detection efficiency and sensitivity. Systematic uncertainties associated with this single-particle detection of BCA are mostly associated with its low-mass detection limit, which results in the need to extrapolate detected BCA to get an estimate of total BCA mass.

[46] The SP2 instrument was flown on the WB-57F high-altitude aircraft from a midlatitude location in November 2004. Data from two flights were analyzed to give size distributions from the boundary layer to the lower stratosphere (18 km) for SA particles in the range 0.17–0.65 μm diameter and for BC particles in the range 3–300 fg mass (0.15–0.7 μm volume equivalent spherical diameter). The boiling point temperature distribution of all ambient incandescing aerosols revealed a single mode, consistent with a composition of BC.

[47] Because of the limited detection-size range of the SP2, total aerosol mass estimates were extrapolated. Total aerosol results were scaled on the basis of typical midlatitude distributions. For BCA it was assumed that mass distributions are adequately represented by a single lognormal distribution. Although this assumption is supported by measurements of the complete size distributions of BCA in limited regions of the atmosphere, it adds unknown uncertainty to the SP2 estimates of mass loadings. Improvements to lower the detection limit of SP mass are being developed, and are expected to reduce this uncertainty.

[48] The SP2 results for BCA mass mixing ratios (MMRs) showed a large gradient in the lower atmosphere, decreasing from 100 ng kg^{-1} near the surface to 1–5 ng kg^{-1} near 5 km altitude. MMR values were nearly constant as a function of altitude above 5 km and there was no clear geographical dependence over the small (10°) ranges of latitude and longitude sampled. BCA values averaged 1.6 ± 1.6 ng kg^{-1} above 5 km. The altitude gradient of total aerosol mass-loading was smaller than that of BCA in the lowest 5 km, and values averaged 480 ± 250 ng kg^{-1} above 5 km. BCA mass fractions decreased with altitude and represented 1% or less of the total aerosol mass above 4 km. Approximately 40% of observed BC particles showed evidence of internal mixing. No evidence of a size-dependent removal of BCA from the atmosphere was observed over the size range of the SP2 or the altitude range explored.

[49] Two global aerosol models (ECHAM4/MADE and LMDzT-INCA) were compared to the SP2 vertical profiles. The models were chosen to reflect the range of results for BCA mass loading in the upper troposphere and lower stratosphere within the AeroCom suite of global aerosol models. The models agree well near the surface but diverge widely for BCA mass and mass fraction in the free troposphere and above. The ECHAM4/MADE model provides the lower model results, which are in good to fair agreement with the SP2 results throughout the profile. The comparison will help resolve the important systematic differences in model processes that determine BCA loadings. Further intercomparisons of models and measurements as presented here will improve the accuracy of the radiative forcing contribution from BCA.

[50] **Acknowledgments.** This work was supported by the NOAA Climate and Global Change Program, the NASA Upper Atmospheric Research Program, NASA Radiation Sciences Program, and the DLR-HGF project Particles and Cirrus (PAZI-2). The authors gratefully acknowledge helpful discussion with Kenneth Kelly, Troy Thornberry, Peter Popp, Timothy Marcy, Ryan Spackman and Daniel Murphy; the essential contributions of the pilots and crew of the NASA WB-57F aircraft and the support staff associated with the Aura Validation Experiment campaign; and instrument design and fabrication support from Richard J. McLaughlin and Michael Schein.

References

Arnott, W. P., H. Moosmuller, and D. F. Rogers (1999), Photoacoustic spectrometer for measuring light absorption by aerosols: Instrument description, *Atmos. Environ.*, *33*, 2845–2852.

Baumgardner, D., G. Kok, and G. Raga (2004), Warming of the Arctic lower stratosphere by light absorbing particles, *Geophys. Res. Lett.*, *31*, L06117, doi:10.1029/2003GL018883.

Blake, D. F., and K. Kato (1995), Latitudinal distribution of black carbon soot in the upper troposphere and lower stratosphere, *J. Geophys. Res.*, *100*, 7195–7202.

Chung, S. H., and J. H. Seinfeld (2002), Global distribution and climate forcing of carbonaceous aerosols, *J. Geophys. Res.*, *107*(D19), 4407, doi:10.1029/2001JD001397.

Chung, S. H., and J. H. Seinfeld (2005), Climate response of direct radiative forcing of anthropogenic black carbon, *J. Geophys. Res.*, *110*, D11102, doi:10.1029/2004JD005441.

Clarke, A. D., et al. (2004), Size distributions and mixtures of dust and black carbon aerosol in Asian outflow: Physiochemistry and optical properties, *J. Geophys. Res.*, *109*, D15S09, doi:10.1029/2003JD004378.

Cooke, W. F., and J. J. N. Wilson (1996), A global black carbon aerosol model, *J. Geophys. Res.*, *101*(D14), 19,395–19,409.

Dentener, F., et al. (2006), Emissions of primary aerosol and precursor gases in the years 2000 and 1750, prescribed data sets for AeroCon, *Atmos. Chem. Phys. Disc.*, *6*, 2703–2763.

Guibert, S., et al. (2005), The vertical distribution of aerosol over Europe—Synthesis of one year of EARLINET aerosol lidar measurements and aerosol transport modeling with LMDzT-INCA, *Atmos. Environ.*, *39*(16), 2933–2943.

Harilal, S. S., et al. (1997), Optical emission studies of C_2 species in laser-produced plasma from carbon, *J. Phys. D*, *30*, 1703–1709.

Haywood, J. M., and V. Ramaswamy (1998), Global sensitivity studies of the direct radiative forcing due to anthropogenic sulfate and black carbon aerosols, *J. Geophys. Res.*, *103*(D6), 6043–6058.

Heintzenberg, J., and D. S. Covert (1984), Size distribution of elemental carbon, sulphur and total mass in the radius range of 10^{-6} to 10^{-4}, *Sci. Total Environ.*, *36*, 289–297.

Hendricks, J., B. Kärcher, A. Döpelheuer, J. Feichter, U. Lohmann, and D. Baumgardner (2004), Simulating the global atmospheric black carbon cycle: A revisit to the contribution of aircraft emissions, *Atmos. Chem. Phys.*, *4*, 2521–2541.

Intergovernmental Panel on Climate Change (2001), *Climate Change 2001: The Scientific Basis—Contribution of Working Group I to the Third Assessment Report of the Intergovernmental Panel on Climate Change*, edited by J. T. Houghton et al., 881 pp., Cambridge Univ. Press, New York.

Jacobson, M. (2000), A physically-based treatment of elemental carbon optics: Implications for global direct forcing of aerosols, *Geophys. Res. Lett.*, *27*(2), 217–220.

Jayne, J. T., D. C. Leard, X. Zhang, P. Davidovits, K. A. Smith, C. E. Kolb, and D. R. Worsnop (2000), Development of an aerosol mass spectrometer for size and composition analysis of submicron particles, *Aerosol Sci. Technol.*, *33*, 49–70.

Jonsson, J. J., et al. (1995), Performance of a focused cavity aerosol spectrometer for measurements in the stratosphere of particle size in the 0.06-2.0-μm-diameter range, *J. Atmos. Oceanic Technol.*, *12*, 115–129.

Jullien, R., R. Botet, and P. M. Mors (1987), Computer simulation of cluster-cluster aggregation, *Faraday Disc. Chem. Soc.*, *83*, 125–137.

Kanakidou, M., et al. (2005), Organic aerosol and climate modeling: A review, *Atmos. Chem. Phys.*, *5*, 1053–1123.

Kjellström, E., J. Feichter, R. Sausen, and R. Hein (1999), The contribution of aircraft emissions to the atmospheric sulfur budget, *Atmos. Environ.*, *33*, 3455–3465.

Koch, D., and J. Hansen (2005), Distant origins of Arctic black carbon: A Goddard Institute for Space Studies model experiment, *J. Geophys. Res.*, *110*, D04204, doi:10.1029/2004JD005296.

Kondo, Y., et al. (2006), Temporal variations of elemental carbon in Tokyo, *J. Geophys. Res.*, *111*, D12205, doi:10.1029/2005JD006257.

Lary, D. J., D. E. Shallcross, and R. Toumi (1999), Carbonaceous aerosols and their potential role in atmospheric chemistry, *J. Geophys. Res.*, *104*(D13), 15,929–15,940.

Lauer, A., J. Hendricks, I. Ackermann, B. Schell, H. Hass, and S. Metzger (2005), Simulating aerosol microphysics with the ECHAM/MADE GCM Part I: Model description and comparison with observations, *Atmos. Chem. Phys.*, *5*, 3251–3276.

Loewenstein, M., et al. (2002), Argus: A new instrument for the measurement of the stratospheric dynamical tracers, N_2O and CH_4, *Spectrochim. Acta, Part A*, *58*, 2329–2435.

Lohmann, U., J. Feichter, J. Penner, and R. Leaitch (2000), Indirect effect of sulfate and carbonaceous aerosols: A mechanistic treatment, *J. Geophys. Res.*, *105*, 12,193–12,206.

Marcolli, C., et al. (2004), Mixing of the organic aerosol fractions: Liquids as the thermodynamically stable phases, *J. Phys. Chem. A*, *108*, 2216–2224.

Möhler, O., et al. (2005), Effect of sulfuric acid coating on heterogeneous ice nucleation by soot aerosol particles, *J. Geophys. Res.*, *110*, D11210, doi:10.1029/2004JD005169.

Moteki, N., Y. Kondo, N. Takegawa, Y. Komanzaki, Y. Miyazaki, and M. Kuwata (2005), Evolution of mixing state and size distribution of black carbon in the urban plumes observed over the ocean, *Eos Trans. AGU*, *86*(52), Fall Meet. Suppl., Abstract A31A-0802.

Murphy, D. M., D. S. Thomson, and M. J. Mahoney (1998), In situ measurements of organics, meteoritic material, mercury, and other elements in aerosols at 5 to 19 kilometers, *Science*, *282*, 1664–1669.

Murphy, D. M., D. J. Cziczo, P. K. Hudson, D. S. Thomson, J. C. Wilson, T. Kojima, and P. R. Buseck (2004), Particle generation and resuspension in aircraft inlets when flying in clouds, *Aerosol Sci. Technol.*, *38*, 400–408.

Ogren, J., P. J. Groblicki, and R. J. Charlson (1984), Measurement of the removal rate of elemental carbon from the atmosphere, *Sci. Total Environ.*, *36*, 329–338.

Penner, J. E., R. E. Dickinson, and C. A. O'Neill (1992), Effects of aerosol from biomass burning on the global radiation budget, *Science*, *256*, 1432–1434.

Petzold, A., H. Kramer, and M. Schonlinner (2002), Continuous measurement of atmospheric black carbon using a multi-angle absorption photometer, *Environ. Sci. Pollut. Res.*, *4*, 78–82.

Pöschl, U. (2002), Aerosol particle analysis: Challenges and progress, *Anal. Bioanal. Chem.*, *375*, 30–32.

Proffitt, M. H., and R. L. McLaughlin (1983), Fast-response dual-beam UV-absorption ozone photometer suitable for use on stratospheric balloons, *Rev. Sci. Instrum.*, *54*, 1719–1728.

Pueschel, R. F., et al. (1992), Black carbon (soot) aerosol in the lower stratosphere and upper troposphere, *Geophys. Res. Lett.*, *19*(16), 1659–1662.

Sato, M., J. Hansen, D. Koch, A. Lacis, R. Ruedy, O. Dubovik, B. Holben, M. Chin, and T. Novakov (2003), Global atmospheric black carbon inferred from AERONET, *Proc. Natl. Acad. Sci. U. S. A.*, *100*(11), 6319–6324.

Schuster, G. L., O. Dubovik, B. N. Holben, and E. E. Clothiaux (2005), Inferring black carbon content and specific absorption from Aerosol Robotic Network (AERONET) aerosol retrievals, *J. Geophys. Res.*, *110*, D10S17, doi:10.1029/2004JD004548.

Slowik, J. G., et al. (2004), Particle morphology and density characterization by combined mobility and aerodynamic diameter measurements. Part 2: Application to combustion-generated soot aerosols as a function of fuel equivalence ratio, *Aerosol Sci. Technol.*, *38*, 1206–1222.

Stephens, M., N. Turner, and J. Sandberg (2003), Particle identification by laser-induced incandescence in a solid-state laser cavity, *Appl. Opt.*, *42*(19), 3726–3736.

Strawa, A. W., et al. (1999), Carbonaceous aerosol (soot) measured in the lower stratosphere during POLARIS and its role in stratospheric photochemistry, *J. Geophys. Res.*, *104*(D21), 26,753–26,766.

Textor, C., et al. (2005), Analysis and quantification of the diversities of aerosol life cycles within AeroCom, *Atmos. Chem. Phys. Disc.*, *5*, 8331–8420.

Twohy, C. H., and M. R. Poellot (2005), Chemical characteristics of ice residual nuclei in anvil cirrus clouds: Evidence for homogeneous and heterogeneous ice formation, *Atmos. Chem. Phys.*, *5*, 2289–2297.

Wilson, J. C., E. D. Blackshear, and J. H. Hyun (1983), The function and response of an improved stratospheric condensation nucleus counter, *J. Geophys. Res.*, *88*, 6781–6785.

K. C. Aikin, S. H. Chung, D. W. Fahey, R. S. Gao, A. O. Langford, K. H. Rosenlof, J. P. Schwarz, T. L. Thompson, D. S. Thomson, and L. A. Watts, Chemical Sciences Division, Earth System Research Laboratory, NOAA, Boulder, CO 80305, USA (joshua.p.schwarz@noaa.gov)

D. G. Baumgardner, Centro de Ciencias de la Atmosfera, Universidad Nacional Autonoma de Mexico, Ciudad Universitaria, 04510, Mexico City, Mexico.

M. Darbeheshti, J. M. Reeves, and J. C. Wilson, Department of Engineering, University of Denver, 2390 South York Street, Denver, CO 80208, USA. (mdarbehe@du.edu)

J. Hendricks, B. Kärcher, and A. Lauer, DLR-Institut für Physik der Atmosphäre, Oberpfaffenhofen, D-82234 Wessling, Germany.

G. L. Kok, Droplet Measurement Technologies Inc., Boulder, CO 80304, USA.

M. Loewenstein, NASA Ames Research Center, Moffett Field, CA 94035, USA.

M. Schulz, Laboratoire des Sciences du Climat et de l'Environnement, Bat 70, F-91191 Gif-sur-Yvette Cedex, France.

J. G. Slowik, Department of Chemistry, Boston College, Chestnut Hill, MA 02467, USA.